Artificial Intelligence-Based Control Design for Reliable Virtual Synchronous Generators

Qianwen Xu, *Member, IEEE*, Tomislav Dragicevic, *Senior Member, IEEE*, Lihua Xie, *Fellow, IEEE*, and Frede Blaabjerg, *Fellow, IEEE*

***Abstract*—Virtual synchronous generator (VSG) is a promising solution for inertia support of the future electricity grid to deal with the frequency stability issues caused by the high penetration of renewable generations. However, the power variation in power electronic interface converters caused by VSG emulation increases the stress on power semiconductor devices and hence has a negative impact on their reliability. Unlike existing works that only consider stability for VSG control design, this article proposes a double-artificial neural network (ANN)-based method for designing VSG inertia parameter considering simultaneously the reliability and stability. First, a representative frequency profile is generated to extract various VSG power injection profiles under different inertia values through detailed simulations. Next, a functional relationship between inertia parameter (H) and lifetime consumption (LC) of VSG is established by the proposed double-ANN reliability model: ANN_t provides fast and accurate modeling of thermal stress in the semiconductor devices from a given operating profile; with the aid of ANN_t, ANN_{LC} is built for fast and accurate estimation of LC for different inertia parameters in the next step. The proposed approach not only provides a guideline for parameter design given a certain LC requirement, but can also be used for optimal design of VSG parameter considering reliability and other factors (e.g., inertia support in this article). The proposed technique is applied to a grid-connected VSG system as a demonstration example.**

***Index Terms*—Artificial intelligence, reliability, stability, virtual inertia, virtual synchronous generators (VSG).**

I. Introduction

THE utilization of renewable energy resources (e.g., PV, wind turbines) as distributed generation (DG) units have attracted great attention all over the world for the environmental friendly requirements [1]. Power electronics converters are widely used as the interfaces for the integration of the DG units into the grid [2]. In the past, grid frequency is regulated by synchronous generators (SGs), which can provide inertia by absorbing or delivering the kinetic energy stored in their rotors and turbines [3]. However, with the high penetration of DG interface converters in the grid, which have very small or no inertia and damping properties, power system inertia is reduced and the frequency stability is becoming a considerable concern [4].

To increase grid inertia and provide frequency support in the future power electronics-based power system, the virtual synchronous generator (VSG) technology has been proposed by mimicking the essential characteristics of the SGs so that the rotating inertia can be emulated in power electronics interface converters [4], [5]. There are various implementations of VSGs in the literature, like virtual synchronous machine [6], VSG [7]–[9], synchronverter [10], synchronous power controller [11], etc. The inertia characteristics emulated by VSGs can contribute to the total inertia of the grid and enhance the transient frequency stability. A prominent feature of VSG is that its parameters (e.g., the virtual inertia constant H and damping factor D) are not constrained by the physical factors as the real SGs; on the contrary, they are control parameters that can be manually designed to have expected dynamic performance. There are several works discussing the parameter design of the VSG. In [8], [11], the closed-loop characteristic equation of the VSG power loop is derived and a relationship between dynamic performance and design parameters (inertia constant and damping coefficient) is developed. In [12], the coupling effect between active power loop and reactive power loop is analyzed and the inertia coefficient is designed based on the small signal model from the perspective of system stability. The authors in [13] discuss the parameter constraints considering stability. In [14], the influences of parameters on the dynamic response of VSGs are investigated, including peak time, settling time and overshoot. However, none of the exisiting works consider the impact of design parameters on reliability of the VSG, which is a critical concern in power electronics-based power systems.

Power electronic converters are reported to be the most unreliable parts in renewable energy systems [15], e.g., wind power systems [16], photovoltaic (PV) power systems [17], and fuel cell power systems [18]. In particular, power semiconductor devices are the most vulnerable links in power electronic converters [15]. Power processing will pose stress on these sensitive

Manuscript received July 16, 2020; revised October 6, 2020 and November 21, 2020; accepted January 2, 2021. Date of publication January 8, 2021; date of current version May 5, 2021. This work was supported by Start Package for Assistant Professor within STandUP Strategic Research Area at KTH, Sweden. Recommended for publication by Associate Editor J. Liu. *(Corresponding author: Qianwen Xu.)*

Qianwen Xu is with the Electric Power and Energy Systems Division, KTH Royal Institute of Technology, 11428 Stockholm, Sweden (e-mail: qianwenx@kth.se,).

Tomislav Dragicevic is with the Department of Electrical Engineering, Technical University of Denmark, 2800 Kongens Lyngby, Denmark (e-mail: tomdr@elektro.dtu.dk,).

Lihua Xie is with the School of Electrical and Electronic Engineering, Nanyang Technological University, Singapore 639798, Singapore (e-mail: elhxie@ntu.edu.sg).

Frede Blaabjerg is with the Department of Energy Technology, Aalborg University, 9220 Aalborg, Denmark (e-mail: fbl@et.aau.dk,).

Color versions of one or more figures in this article are available at https://doi.org/10.1109/TPEL.2021.3050197.

Digital Object Identifier 10.1109/TPEL.2021.3050197

devices, affect their lifetimes and finally impact system reliability. Previously, reliability assessment is achieved in a statistic way assuming constant failure rates regardless of their mission profiles and MIL-HDBK-217 handbook has been widely adopted to predict lifetime of power electronic devices [19], [20]. Recent trend in reliability of power electronics systems is moving toward physics-of-failure based reliability assessment by identifying root-causes of failures [16], [18], [21]–[26]. The authors in [21] and [22] present experimental validation of linear cumulative damage theory in the lifetime prediction of power semiconductor devices. In [23], a comprehensive review of failure and lifetime prediction of power devices is presented, which summarizes different techniques typically used for measuring the junction temperature for lifetime prediction. The authors in [16] proposes a mission profile based system level reliability analysis of dc/dc converters for a fuel cell power application. The authors in [24] propose a reliability oriented design of modular multilevel converters for medium-voltage static synchronous compensator. In [25], a thermal stress based design of smart transformer is proposed. Reliability oriented design tools are development for PV converters in [17] and [26]. In [18], selection of power converters in double-fed induction generator (DFIG) wind turbine is presented with enhanced system-level reliability. For all the state-of-art reliability works [15], [17], [20]–[25], failures of power semiconductor devices are mainly induced by thermal stress and are assessed by mean junction temperature and junction temperature cycles over the operating period. The power loading and ambient temperature profiles are normally considered as mission profiles of power semiconductor devices, as they have direct contribution to the thermal stress. Lifetime consumption (LC) of a power semiconductor device is estimated using the obtained junction temperature profile from thermal stress under a specific mission profile, which requires detailed simulations or experiments. To assist long-term simulation, a lookup table method is conventionally applied to transform the mission profile into thermal cycles for LC estimation [17], [26]. However, as the lookup table method is based on linear interpolation, it cannot learn the nonlinear relationship between the input and output data; moreover, it is not suitable for high dimensional data mapping, which is inevitable when impact of both system design parameters and mission profile on the system's lifetime needs to be studied. A promising solution to overcome the drawbacks is to use an artificial neural network (ANN), which has the capability to approximate nearly any functions of input/output data with arbitrary precision [27], [28]. Inspired by wide applications of ANN in prediction [28], [29], it is possible to use ANN to map LC of power semiconductor device from various mission profiles to achieve faster and more accurate LC estimation.

The VSG technology is important for inertia support in the future power electronics based power systems. By controlling the DG interface inverters as VSGs to enhance grid inertia and provide frequency support, the loading profiles of VSGs will be different from the original loading profiles. This will affect LC of power semiconductor devices in the DG interface inverters, which are commonly designed based on the original loading conditions (i.e., power outputs of DGs) without considering inertia support. Current methods for parameter design of VSGs only consider system dynamics and stability, while their impacts on power electronics reliability are not taken into consideration. As power semiconductor devices are normally the weakest links in the power electronic converter systems, the LC of power semiconductor device is selected as the system reliability metric. In this article, we propose a double-ANN-based approach for designing a more reliable grid connected VSG system with the consideration of both inertia (stability) and LC (reliability). First, a representative frequency profile is extracted to generate different power injection profiles under different control parameters (i.e., inertial constant H). Then a double-ANN model is built to map H to LC; ANN_t is constructed and trained to translate mission profiles (power injection profile and ambient temperature profile) into the thermal loading profile based on detailed simulation data. Based on ANN_t and the generated power injection profile under different values of H, LC of power semiconductor device in DG inverter is calculated, and these data are used to train ANN_{LC}, which models the relationship between input data (H) and output data (LC). ANN_{LC} provides a quick estimation of LC given different inertia parameters. Then the overall system optimization function for parameter design is formulated with the combined objectives of inertia and LC. The main contributions of this article are summarized as follows.

1) Unlike conventional VSG design methodologies only considering inertia, it optimizes the control parameter considering both inertia performance and LC.
2) A double-ANN model is proposed to provide a quantitative relationship for how the designed inertia parameter will impact reliability.
3) A novel profile reduction method is developed to map a long-term mission profile to a representative short-term mission profile with the same stochastic features.
4) A guideline is developed about how to optimize the control parameter considering LC and other performance factors (e.g., the inertia requirement and the transient stability requirement) simultaneously.

The rest of this article is organized as follows. Section II describes VSG system model and the impact of inertia parameter. The double-ANN-based technique is proposed for VSG parameter design by simultaneously considering stability and reliability in Section III. The proposed technique is demonstrated and verified in Section IV by a case study. Finally, the conclusion is drawn in Section V.

II. System Description and Inertia Design

There are several different implementations of the VSG. In this article, a relatively common topology is adopted, as shown in Fig. 1 [5], [31]. An energy storage unit is applied with the VSG control technique to mimic the swing equation of the SGs in order to support the grid frequency fluctuation and provide inertia. A typical three phase voltage source inverter is connected to the grid at the point of common coupling through an LC filter L_f and C_f. Grid impedance is denoted as Z_g. The inverter

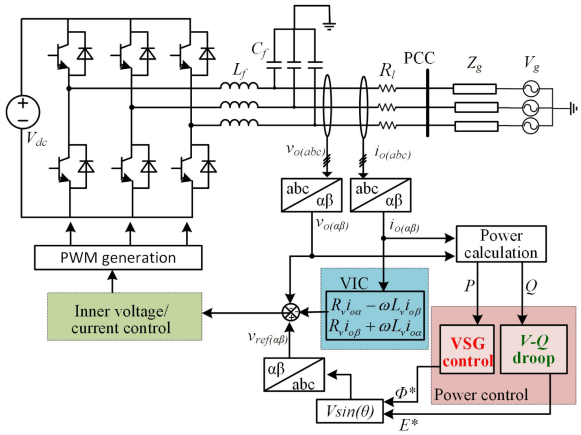

Fig. 1. Grid-connected VSG system.

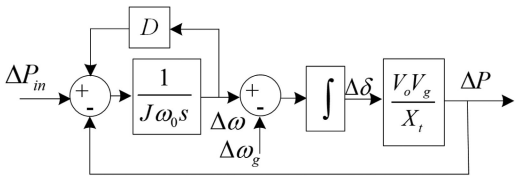

Fig. 2. Small signal model of the grid connected VSG system.

operates in the voltage source mode with the inner voltage and current regulation using PR controllers in synchronous reference frame. The virtual impedance control (VIC) is implemented to emulate an impedance connected in series with the grid line impedance between the inverter output and the PCC to make the equivalent line impedance inductive [30]. The VSG control is implemented in the power control loop to provide virtual inertia, damping and droop control. As only one VSG is studied here, droop control is not included in VSG control block.

In various implementations of VSG control, the mimicking of rotor inertia is similar but the forms of damping vary, e.g., $D(\omega-\omega_0)$ and $D(\omega-\omega_g)$ [5], [31], where D is the damping factor, ω_0 is the nominal angular frequency, ω_g is the grid angular frequency. Note that the former one combines droop and damping, while the latter considers separate droop and damping terms. Here, $D(\omega-\omega_g)$ is adopted as an application example, as its damping factor will not impact droop coefficient, and thus, it can be designed to get desired system dynamics. The swing equation is expressed as

$$P_{in} - P - D(\omega-\omega_g) = J\omega\frac{d(\omega-\omega_g)}{dt} \tag{1}$$

where P_{in} is the set-point value of active power, P is the measured output power of VSG, ω is the angular frequency of the virtual rotor, J represents the moment of inertia of the virtual rotor; as the deviation of ω is relatively small, and $J\omega$ can be approximated by $J\omega_0$ [8].

The small signal model of the VSG system in Fig. 1 is shown in Fig. 2 [8]. Then the transfer function from power reference to the output power is derived as

$$\Delta P = \Delta P_{in}\frac{\frac{V_o V_g}{X_t J\omega_0}}{s^2 + (\frac{D}{J\omega_0})s + \frac{V_o V_g}{X_t J\omega_0}} \tag{2}$$

where X_t is the equivalent inductive line impedance considering the virtual impedance.

The transfer function is equivalent to a standard second-order differential equation [8]

$$\Delta P = \Delta P_{in}\frac{\omega_n^2}{s^2 + 2\xi\omega_n s + \omega_n^2} \tag{3}$$

with the natural frequency ω_n and damping ratio ξ expressed as $\omega_n = \sqrt{\frac{V_t V_g}{X_t J\omega_0}}$ and $\xi = \frac{D}{2\sqrt{\frac{V_t V_g J\omega_0}{X_t}}}$.

Based on (3), J and D can be tuned to have the desired dynamic response. Given a specific inertia J and the required damping ratio ξ, D can be designed as

$$D = 2\xi\sqrt{\frac{V_t V_g J\omega_0}{X_t}}. \tag{4}$$

The variables in (1) are transformed into per-unit values so that the system dynamic response is not constrained by the power ratings of power converters, i.e., frequency response of a 1 MVA system will be the same as that of a 1-kVA system as long as their parameters are equivalent in per-unit forms [32]

$$P_{in\_pu} - P_{pu} - D_p(\omega_{pu} - \omega_{g\_pu}) = 2H\frac{d(\omega_{pu} - \omega_{g\_pu})}{dt} \tag{5}$$

where $H = \frac{J\omega_0^2}{2S_N}$, $D_p = \frac{D\omega_0}{S_N}$, and S_N is the power rating of the DG.

Once the inertia constant H is determined, the corresponding J and D can be derived according to (4) and (5) to have expected system dynamics. Therefore, we assume that H is the only control parameter to be designed.

Fig. 3 shows the dynamic response of a VSG to support the grid frequency variation with different inertia values. At 3 s, the grid frequency ramps down from 50 to 49.8 Hz with the rate at

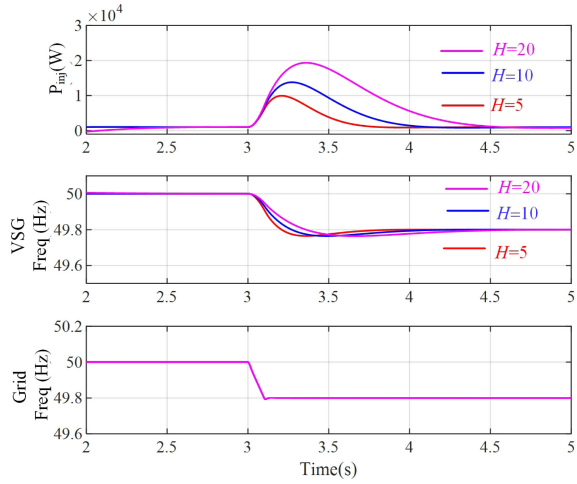

Fig. 3. Dynamic response of a VSG to support the grid frequency variation with different H.

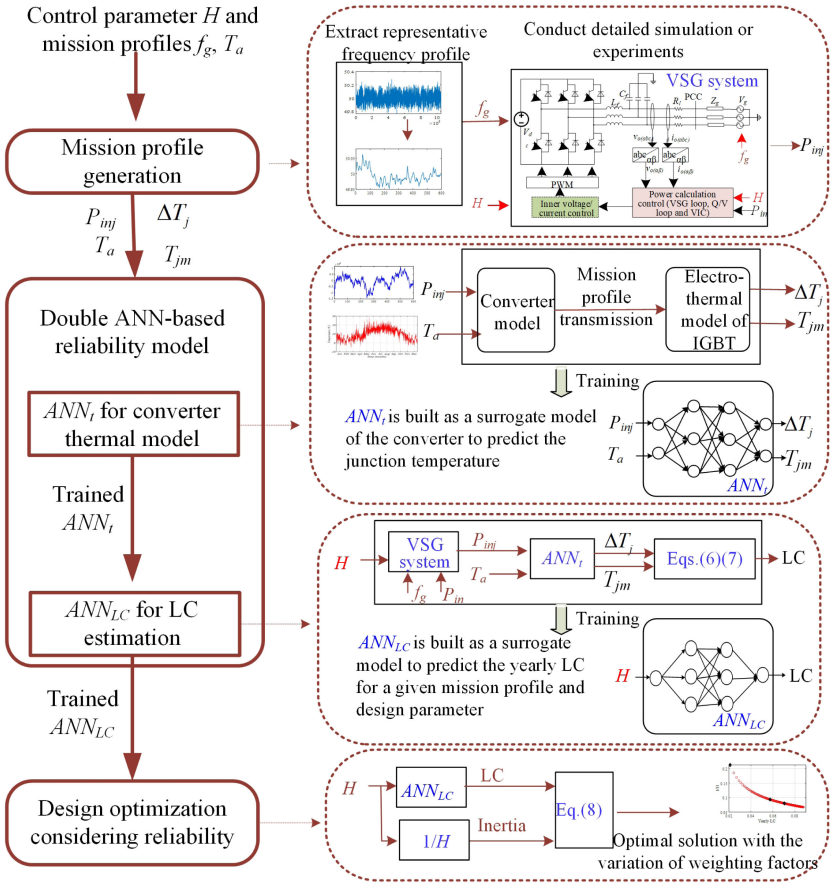

Fig. 4. Proposed double-ANN framework.

2 Hz/s. The VSG is to provide inertia support of the grid. As can be observed, a larger H will provide a larger inertia support, and thus a larger H is expected from inertia's perspective. However, a larger H also means more energy extracted from the energy source for inertia support, as shown in the response of power P in the first plot of Fig. 3. The plot reveals that the VSG has different power outputs with different values of H for different levels of inertia support, which will definitely impact the LC of power devices in the VSG and finally impact the reliability of the VSG. Therefore, it is clear that H is a key parameter that affects both inertia and reliability.

In existing works, there are no general rules for designing H. Some works select H based on parameters from the conventional SGs (0–10 s) [4], or from stability [10]–[13]. But none of them consider reliability. Therefore, an ANN-based methodology is proposed to provide a quantitative relationship of inertia parameter and reliability, and develop a guideline for the optimal design of H considering both stability and reliability.

III. Proposed Double-ANN Design Approach

Fig. 4 shows the proposed double-ANN framework for designing a grid connected VSG system, which involves representative mission profile generation, double-ANN-based LC modeling and design optimization considering both reliability and inertia.

A. Representative Mission Profile Generation

The LC of power semiconductor device is significantly influenced by the system operating conditions, e.g., the loading profile and ambient temperature profile. Unlike the original renewable energy sources, which normally operate at maximum power point tracking mode or power control mode, a VSG will provide extra power injection to support system inertia during the grid frequency fluctuations. This extra injected power passes through the grid connected inverter, increases power loss and thermal stress, and as a result, causes increased LC. Thus, the power injection profile P_{inj} of VSG consists of the original power set-point value P_{in} and the extra power injection caused by virtual inertia support. With different values of H, different loading profiles P_{inj} will be generated and consequently, the LC will be affected.

A problem encountered in this step is to get the power injection profile from a detailed simulation over a long period with the grid frequency profile. This is because of the long simulation time required for simulating a detailed simulation model over a long operating period, e.g., for a one-minute operating period, the simulation running time is almost 1 min.

To avoid running lengthy numerical simulations, the long-term frequency profile can be represented by a short-term frequency profile that has similar statistical properties. Based on Kolmogorov–Smirnov (K–S) test result for the long-term frequency profile, the data follows the standard normal distribution. For the normal distribution, the statistical properties are determined by the mean value and standard deviation [33]. To be representative, the short-term frequency profile is generated to have the same normal distribution properties as the long-term frequency profile. Then the short-term frequency profile is applied to the system in Fig. 1 with various values of H to generate the power injection profile of VSG.

B. Double-ANN LC Model

After the power injection profiles of VSG for different H constants are obtained, they are applied to the ANN-based power semiconductor converter thermal model in order to estimate the LC of the power devices.

The main failure mechanism of power device is related to the thermal cycling, which is translated from the mission profiles and can lead to wear-out failures, e.g., bond wire lift off. In a standard design for reliability approach, the lifetime evaluation involves translation of the mission profile to thermal loading profile, interpretation of thermal loading profile and LC modeling. To assist the simulation for the LC with a long-term mission profile (e.g., an annual mission profile), a lookup table model is normally constructed to translate the mission profile to thermal loading profile. However, as the electrothermal model is nonlinear, to enhance the accuracy of lookup table method, numerous simulations are required to have more breakpoints in the lookup tables; and the whole process for estimating LC of power electronic converters usually consists of several lookup tables (e.g., one lookup table for device model, one lookup table for power loss model and one lookup table for thermal model in [26]). Thus, the process to build an accurate lookup table based model is quite complicated, requiring the knowledge of inner physical models [26]. And when a large amount of data are processed, lookup table-based method is still time-consuming.

As a widely used machine learning algorithm, ANN offers a promising solution for dealing with nonlinear relationships with a large amount of data [28]. In the following parts, a double-ANN-based approach is used for fast and accurate mapping of the relationship from control parameter H to LC.

1) ANN$_t$: First, ANN_t is constructed to translate the mission profiles (power injection profile and ambient profile) into the thermal loading profile.

An ANN is based on a collection of artificial neurons, which models the neurons in a biological brain. The neurons receive input, change their internal state (activation) according to that input, and produce output depending on the input and activation. A general multilayer feedforward ANN consists of an input layer, one or more hidden layers and an output layer, where each layer has several neurals. The basic knowledge of an ANN is illustrated in Appendix. For ANN_t, it has two neurons in the input layer (for two input variables: power injection P_{inj} and ambient temperature T_a) and two neuron in the output layer (for two output variables: mean junction temperature T_{jm} and cycle amplitude ΔT_j). The hidden layers can be determined by trial and error from training and test data. Fig. 5 shows an example of ANN_t.

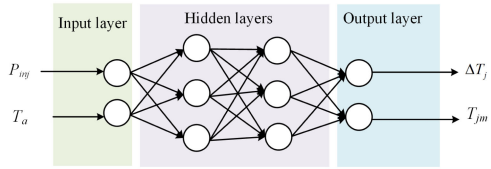

Fig. 5. Structure of ANN_t.

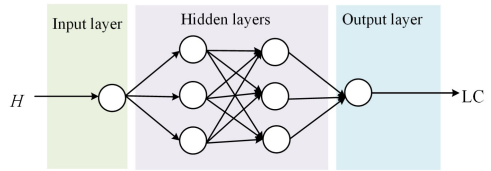

Fig. 6. Structure of ANN_{LC}.

The training and test data of ANN_t are obtained by simulating the detailed models of power converter with the associated thermal model. The mission profiles of power injection and ambient temperature are taken as the input variables of the ANN_t and the resulted junction temperature variation profile is the output.

2) ANN$_{LC}$: Next, ANN_{LC} is built to estimate the LC according to different values of H.

Similar as ANN_t, ANN_{LC} is a multilayer feedforward ANN. It has one neuron at input layer (for virtual parameter H) and one neuron at output layer (for LC), as shown in Fig. 6.

The training and test data of ANN_{LC} are datasets of H and the corresponding LC. Given different values of H, the corresponding LC is estimated based on the following procedure.

As described in Section III-A, power injection profiles P_{inj} are obtained by simulating VSG system in Fig. 1 with various selections of H under the representative short-term frequency profile. Then the power injection profile P_{inj} and ambient temperature profile T_a are fed to ANN_t to generate the junction temperature profile T_j.

The junction temperature profile provides information of the mean junction temperature T_{jm}, cycle amplitude ΔT_j, and cycle period t_{on}. As the junction temperature profile usually contains mission profile dynamics, which is irregular, a cycle counting algorithm such as a rainflow analysis is needed for the thermal cycling interpretation [17], [26]. For example, the rainflow counting algorithm can decompose an irregular profile into several regular cycles according to the amplitude value ΔT_j, average value T_{jm} and period of the cycle t_{on}. By applying this method to the junction temperature profile, the number of cycles at a certain cycle amplitude ΔT_j, mean junction temperature T_{jm}, and cycle period t_{on} can be obtained.

TABLE I
LIFETIME MODEL PARAMETERS OF AN IGBT MODULE

Variables	Value
A	$3.4368 * 10^{14}$
α	-4.923
β_0	1.942
β_1	$-9.012 * 10^{-3}$
C	1.434
β_1	-1.208
f_d	0.6204
a_r	0.28
E_a	0.06606eV
k_b	$8.6173324 * 10^{-5} eV/k$

TABLE II
SYSTEM PARAMETERS

Variables	Description	Value
V_{dc}	Input voltage	650V
V_{ac}	Grid voltage	220V
f_s	Switching frequency	5kHz
ω_0	Nominal angular frequency	50Hz
L_f, C_f	LC filter	1.8mH,0.25mF
L_v, R_v	Virtual impedance	4mH,0Ω
k_{pv}, k_{rv}	Voltage controller	2,100
k_{pc}, k_{rc}	Current controller	10,100
S_N	Power rating	50kW
ξ	Damping ratio	0.707

With the obtained information, the number of cycles to failure is estimated as [17]

$$N_f = A \times (\Delta T_j)^{\alpha} \times (ar)^{\beta_1 \Delta T_j + \beta_0} \times \left[\frac{C + (t_{on})^{\gamma}}{C+1}\right] \exp\left(\frac{E_a}{k_b \times T_{jm}}\right) \times f_d \quad (6)$$

where N_f is the number of cycles to failure. T_{jm} is the mean junction temperature, ΔT_j is the cycle amplitude, and t_{on} is cycle period, which are obtained from the cycle counting method. Other coefficient parameters are given in Table I.

Based on Miner's rule [17], the LC of the power device is obtained as

$$LC = \sum_i \frac{n_i}{N_{fi}} \quad (7)$$

where n_i is the number of cycles for a certain ΔT_j, T_{jm}, and t_{on}, which is obtained from the rainflow analysis, and N_{fi} is the number of cycles to failure for the specific stress condition. For instance, if the number of cycles n_i is counted from a one year mission profile, the corresponding LC will represent a yearly LC of the power device. When the value of LC accumulates to unity (i.e., 100%), the power electronics device is considered to fail.

By following the procedure described above, ANN_{LC} can be constructed with the input data (H) and corresponding output data (LC).

C. Optimization Model Considering Both Inertia and LC

The trained ANN_{LC} maps the control parameter H to yearly LC, which provides the basis for optimal parameter design of H considering both reliability and inertia.

As discussed, the control parameter H impacts both inertia and LC and we want to optimize H from the perspective of reliability and inertia simultaneously. One objective is to minimize LC, which can be directly obtained by ANN_{LC} given different values of H. From the inertia's perspective, the mechanism for inertia enhancement is essentially increasing H [4]. Therefore, another optimization objective is selected as the maximization of H, or equivalently, minimization of $1/H$. Thus, the overall cost function for optimizing H with inertia and reliability is formulated as

$$f(H) = LC^2 + w_1 \left(\frac{1}{H}\right)^2 \quad (8)$$

where w_1 is the weighting factor to balance the importance between the two terms and is a user-defined parameter based on the customer requirement.

By solving $f(H)$, the optimal H can be obtained considering both LC and inertia with different values of weighing factor w_1.

It should be mentioned that, the cost function in (8) can be revised by taking more factors into consideration. For example, system dynamic performance indices related to inertia, such as RoCoF, frequency nadir and settling time [4], can also be selected as optimization terms.

This method is also flexible for the design of other control parameters considering reliability, like droop control parameter. The study of droop control parameter with LC is briefly discussed in Appendix B.

IV. CASE STUDY

The proposed methodology in Fig. 4 is applied to a grid-connected VSG system in Fig. 1 as a demonstration example. The system parameters are listed in Table II. Here the damping ratio ξ is selected as 0.707 as it offers a good compromise between rise time and settling time [39].

The proposed method is applied in the VSG system in Fig. 1 as an application example, and the detailed procedure described in Section III and Fig. 4 is demonstrated.

A. Representative Mission Profile Generation

A representative mission profile is generated to shorten the simulation time. Fig. 7(a) shows one-month grid frequency profile in Great Britain [34] with 1 s resolution. Its normal distribution is shown in Fig. 7(b). with a mean of 49.9995 Hz and standard deviation at 0.062. To get a representative short-term frequency profile, a 10-min frequency profile is generated with the same statistical properties as Fig. 7. The generated representative frequency profile is shown in Fig. 8(a) with its normal distribution in Fig. 8(b). Then, a yearly frequency profile can be generated using the short-term frequency profile.

The generated frequency profile is fed into the system described in Fig. 1 with the variation of H to generate the power injection profiles P_{inj} of VSG system. Fig. 9 shows simulation results of total power injection of VSG P_{inj}, the original power set-point profile P_{in}, VSG frequency and grid frequency with H selected to be 10 as an example. Note that P_{in} is usually given by the operator, here it is given as the second plot in Fig. 9

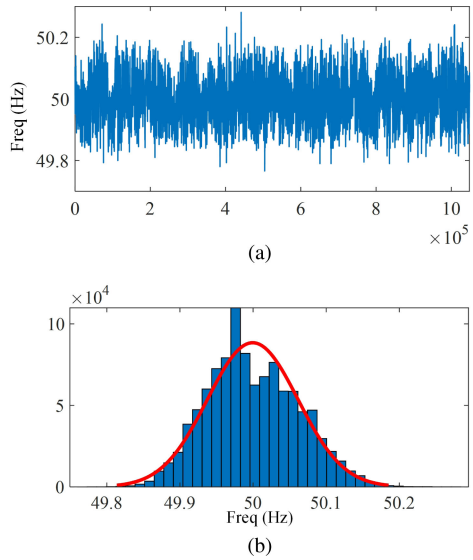

Fig. 7. One-month grid frequency profile in Great Britain with its normal distribution.

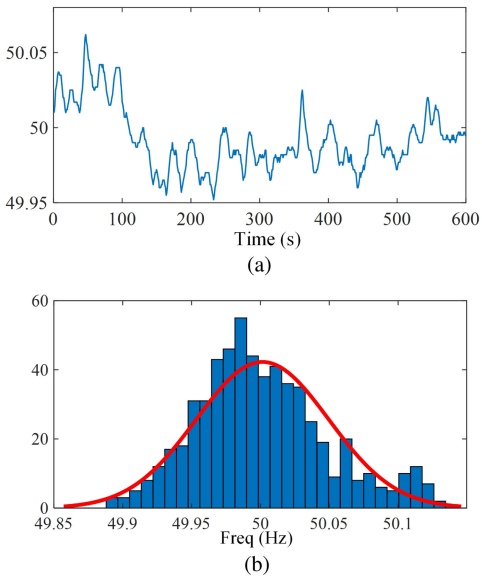

Fig. 8. Generated representative frequency profile with its normal distribution.

as an example. As can be observed, with frequency fluctuations, VSG injects or absorbs extra power accordingly to supply inertia.

B. Double-ANN Model Training

Double-ANN model is trained based on data from detailed simulations using the feedforward neural network model.

1) ANN$_t$: ANN_t is constructed according to Section III-B1. Numerous simulations of the power converter model are conducted with the input data sweeping at $P_{inj} = 50 : 50 : 1000$(W) and $T_a = -10 : 5 : 40$ to generate the corresponding output data of T_j. There are 231 (i.e., 21*11) sets of input/output

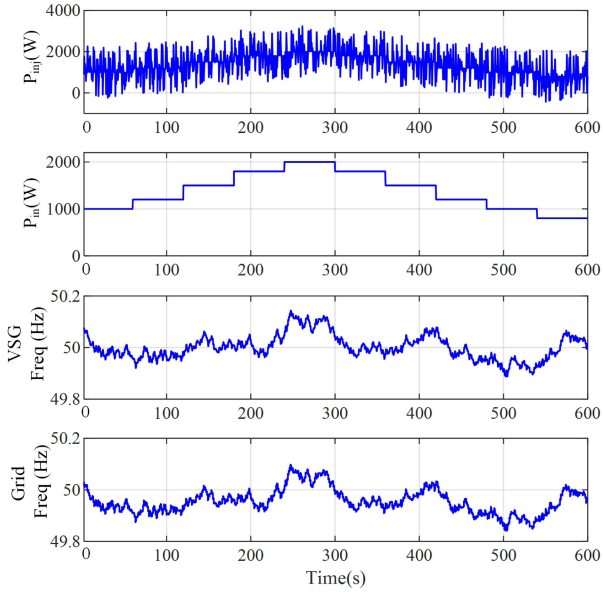

Fig. 9. Simulation results of power injection of VSG P_{inj}, the original power set-point profile P_{in}, VSG frequency and grid frequency with H selected to be 10.

data. The training data are normalized and fed to a feedforward neural network model in deep learning toolbox in Matlab to get ANN_t. To determine the structure of ANN_t, training results are compared for different ANN structures with one or more hidden layers and different numbers of neurons in each layer. In this study, the number of hidden layers is selected to be three neurons in both hidden layers, which is the simplest network that provides excellent performance.

2) ANN$_{LC}$: ANN_{LC} is constructed according to Step III.B2. Given different values H (2:1:20), corresponding 19 sets of power injection profile P_{inj} are obtained, as described in Section IV-A. The ambient temperature is another mission profile that impacts LC of power device. Considering that our focus is the impact of power injection profile, ambient temperature is fixed at 20 °C. The mission profiles P_{inj} and T_a are next fed into ANN_t to get the thermal cycling profile T_j immediately. Then the rainflow counting algorithm is applied to get the number of cycles at a certain cycle amplitude, mean junction temperature and cycle period. The yearly LC of the power device in VSG inverter is calculated based on (6) and (7).

The structure of ANN_{LC} is determined by following the same procedure as ANN_t. Taking values of H (2:1:20) as input and corresponding LC values as output data of ANN_{LC}, doing normalization and feeding them into a feedforward ANN, ANN_{LC} is trained.

C. Design Optimization Considering Reliability

The trained ANN_{LC} can be used for selecting control parameter given a certain LC requirement. Fig. 10 presents the yearly LC of the VSG with different selection of H (2:0.1:20). It shows that LC increases with the increase of inertia parameter.

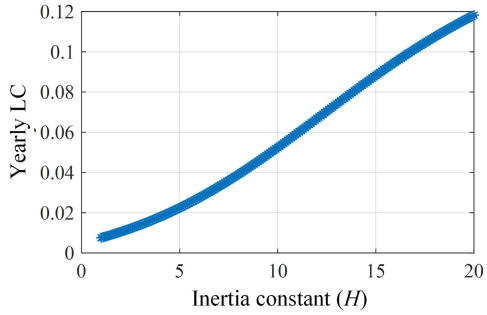

Fig. 10. Yearly LC of the VSG with different values of H (2:0.1:20).

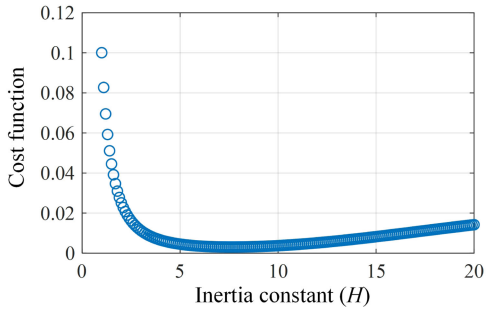

Fig. 12. Cost value with the variation of inertia value H when weighting factor is selected at 0.1.

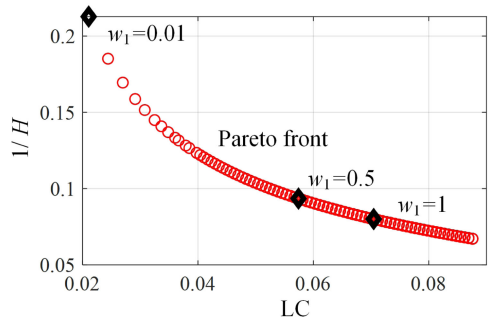

Fig. 11. Optimal yearly LC and reciprocal of inertia ($1/H$) with the sweeping of w_1 at 0.01:0.01:1.2.

If reliability requirement of the yearly LC is less than 0.03, H should be selected less than 6.

The trained ANN_{LC} can also be applied for design optimization considering LC and inertia using (8), as illustrated in Section III-C and Fig. 4. To solve the cost function in (8) is equivalent to solve a multiobjective problem. To solve a multiobjective problem, the simplest and most common approach is the weight-sum method, achieved by multiplying each objective function by a weighting factor and summing up all weighted objective functions [35]. The weighting factors are usually scaled to make their summation to be one. The relative value of the weights generally reflects the relative importance of the objectives. The weights can be used in two ways. The designer may either set the weighting factors to reflect preferences before the problem is solved, or systematically alter weights to yield different Pareto optimal points.

Here, as the problem is a two-objective problem, for simplicity, we set the weighting factor of LC^2 as 1 and the weighting factor of $(1/H)^2$ as w_1 in (8), so we only have one weighting factor w_1 to be altered. By alternating w_1 value, we can get the Pareto front of the feasible space of the problem (8), denoted as red line in Fig. 11, which is a set of optimal solutions under different values of w_1 ($w_1 = 0.01{:}0.01{:}1.2$). Three optimal points corresponding to $w_1 = 0.01$, 0.5 and 1 are highlighted in Fig. 11 as an example to show the balance between LC and inertia with different values of w_1. With the increasing weight in inertia, a larger optimal inertia value (i.e., smaller $1/H$) is obtained, while this results in an increase of LC. For example, if we want to ensure the LC to be less than 0.06, and to maximize the inertia, we can select inertia as 11 (i.e., $1/H = 0.09$), the corresponding w_1 is around 0.5. Therefore, if inertia support capability is more important, we can select the H based on Fig. 11 to have optimal inertia support capability with guaranteed requirement of LC.

Fig. 12 shows the cost value with the variation of inertia value H when weighting factor is selected at 0.1. The optimal solution of H for this weighting factor can be obtained by finding the lowest value in the plot, which can then be applied for parameter design of VSG.

To compare the lookup table method and the proposed method for reliability evalution, a lookup table based model is built based on [26] consisting of three lookup tables (one lookup table for device model, one lookup table for power loss model and one lookup table for thermal model). The lookup table method and the proposed method are conducted in Matlab in a laptop with an Intel i7-8550 CPU and 8 GB of RAM. For the lookup table method, the running time under the 600 s power injection profile is 125.670926 s. For the proposed method, the running time is 14.249055 s, which reduces 89% computational time. Therefore, the lookup table method is more complicated to build and has much higher computational time. While for our method, we only need to know input and output data obtained from simulations, and we can obtain fast and accurate results.

D. Experimental Verification for Inertia Support

Hardware in the loop experiments are conducted in RT-lab OP5600 Simulator platform in Energy Research Institute @ NTU to verify the control parameter design for inertia providing capability. The same parameters listed in Table II are adopted. Fig. 13 shows the experimental result for the inertia constant H selected at 10, when the active power reference steps up from 500 W to 2 kW and steps down from 2 kW to 500 W. Fig. 14 shows the result with the same variation for inertia constant H selected at 2. It shows that, a higher inertia constant H will have more smooth frequency variation, and the maximum frequency deviation during transient is much smaller, which verifies the design goal of inertia that a higher inertia constant H will lead to higher inertia support.

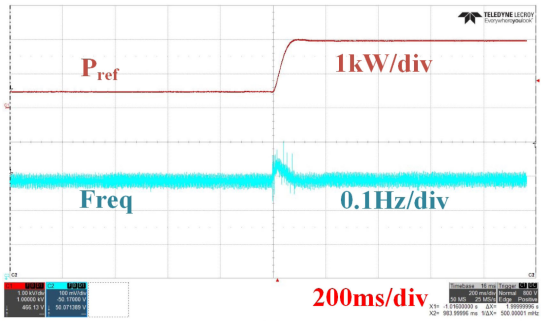

(a)

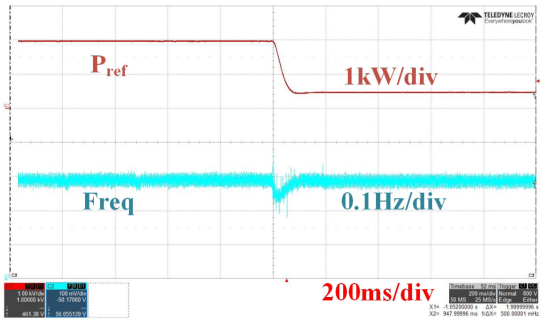

(b)

Fig. 13. Experimental result for inertia constant H selected at 10. (a) When the active power reference steps up from 500 W to 2 kW. (b) When the active power reference steps down from 2 kW to 500 W.

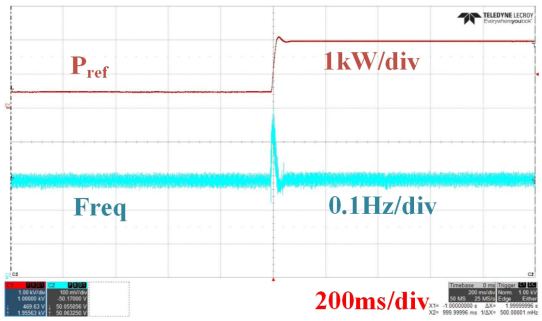

(a)

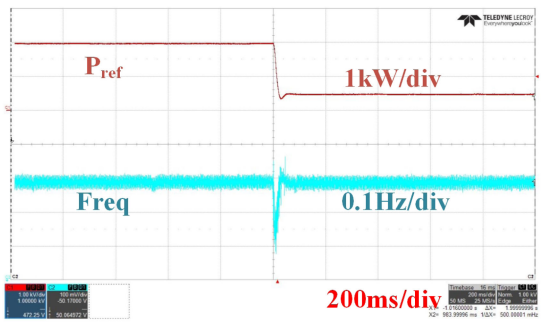

(b)

Fig. 14. Experimental result for inertia constant H selected at 2. (a) When the active power reference steps up from 500 W to 2 kW. (b) When the active power reference steps down from 2 kW to 500 W.

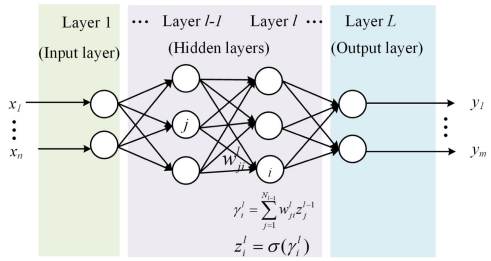

Fig. 15. General structure of an ANN.

V. Conclusion

Unlike existing VSG works that only considers stability, this article proposes a double-ANN-based method for designing VSG inertia parameter (H) considering both reliability and stability. First, a representative frequency extraction method is proposed to avoid numerous lengthy simulations for generating power injection profiles under different inertia parameters. Next, a double-ANN reliability model is constructed for fast and accurate estimation of LC of power device. Finally, the trained double-ANN model is combined with the other performance factors (such as inertia in this article as an example) to formulate the cost function for optimal design of inertia parameter. The proposed approach is applied in a grid-connected VSG system as a demonstration example. It provides a guideline about how the inertia constant should be selected within the acceptable damage in device reliability. It could also help the system operators to develop a business model in the future for converter inertia support considering reliability and other performance factors.

Appendix

A. Basic Knowledge of ANN

An ANN is based on a collection of artificial neurons, which models the neurons in a biological brain. A typical ANN structure consists of two basic types of components—the neurons for processing information and the links for interconnections. The feedforward multilayer network structure is a commonly used structure for ANN [27]. Assume there are L layers. The first layer is called the input layer, which consists of n neuros ($n =$ the number of input variables). The last layer is called the output layer, which consists of m neurons ($m =$ the number of output variables). The rest layers, i.e. layers 2 to $(L-1)$, are hidden layers. Let the number of neurons in the lth layer be N_l, $l = 1, 2,.., L$. Define the parameter w_{ji} to represent the weight of the link between the jth neuron in the $(l-1)$th layer and the ith neuron in the lth layer. Fig. 15 presents a general structure of an ANN.

Each neuron processes the information in two steps [28]. First, collect the information from the neurons from the previous layer, given by

$$\gamma_i^l = \sum_{j=1}^{N_{l-1}} w_{ji}^l z_j^{l-1} \tag{A1}$$

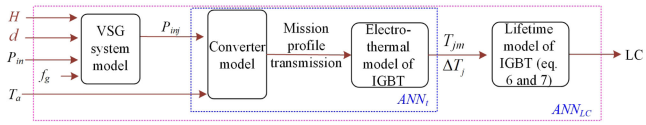

Fig. 16. Procedure of calculating LC of power converters with the variation of droop coefficient d and inertia constant H.

where γ_i^l is the weighted sum information for the ith neuron in the lth layer, which can be seen as the input for that neuron; N_l is the number of neurons in the lth layer, $l = 1, 2,.., L$; w_{ji}^l is the weight of the link between the jth neuron in the $(l-1)$ th layer and the ith neuron in the lth layer; and z_j^{l-1} represents the output of jth neuron in the $(l-1)$ th layer.

Second, the weighted sum information in (A.1) is processed by an activation function to get the final output of the neuron as z_i^l, given by

$$z_i^l = \sigma(\gamma_i^l). \tag{A2}$$

The activation function $\sigma(\cdot)$ can be selected as Sigmoid, Tanh, ReLU, Softmax, etc. Here, the widely used sigmoid function is selected, which is given by

$$\sigma(\gamma) = \frac{1}{1+e^{-\gamma}}. \tag{A3}$$

Then, the output the neurons in the lth layer will be fed to the neurons in the next layer for process.

With the input vector $(x_1, .., x_n)^T$, the process of ANN for prediction can be summarized as [28]

$$\begin{aligned} &z_i^1 = x_i, i = 1, 2, .., N_1 \quad N_1 = n \\ &z_i^l = \sigma\left(\sum_{j=1}^{N_{l-1}} w_{ji}^l z_j^{l-1}\right), i = 1, 2, .., N_l \\ &y_i = z_i^L, i = 1, 2, .., N_L \quad N_L = m \end{aligned} \tag{A4}$$

where $(y_1, .., y_m)^T$ is the predicted output vector of ANN.

To get a proper ANN model to solve the problem, a suitable number of hidden layers and neurons should be selected first. In general, the choice of hidden layers depends on the characteristic of data. More hidden layers are adopted to characterize more complex relationship, yet more data are also required [36]. How to select the number of hidden neurons remains an open question, and they are selected based on experience or the trial and error process, by trying different neurons during training process to get an acceptable accuracy.

The training process of ANN is to use training data to obtain a proper set of weight parameters w_{ji}^l to minimize the estimation error of ANN output variables with the real output variables. The properness is evaluated by a loss function, which is usually a mean-square-error function. The backpropagation training algorithm is widely adopted to get a proper set w_{ji}^l [37]. The training process of ANN can be achieved by many software packages, like Deep Learning Toolbox in Matlab, Kares, pytorch, and tensorflow. In our work, Deep Learning Toolbox in Matlab is used [38]. By feeding the input data and real output data as the training data into the ANN, we can get a well-trained ANN model.

B. Extension of the Proposed Method Considering Droop Parameter Impact on Reliability

This method is flexible to be extended to study the impact of other control parameters (e.g., droop parameter) on reliability. The study of droop parameter is the same as the procedure for H in Fig. 2. First, we can have different droop parameters to run the simulation and get the power injection profiles P_{inj}, and then we feed the power injection profiles P_{inj} to ANN_t to get the thermal profile and calculate the corresponding LC. Then we can build the relationship between input (i.e., droop coefficient d and inertia constant H) and output (i.e., LC) to train ANN_{LC}. The procedure is described in Fig. 16. The training process is similar as to be described in Section IV-B. Therefore, the proposed double-ANN method can be extended to study the impact of droop parameters on reliability, and we can also achieve reliability oriented droop parameter design. As the focus of this work is to study the impact of VSG inertia emulation on reliability, the study of droop parameter is not emphasized.

REFERENCES

[1] M. H. Bollen, "The smart grid: Adapting the power system to new challenges," *Synthesis Lectures Power Electron.*, vol. 2, no. 1, pp. 1–180, 2011.
[2] F. Blaabjerg, R. Teodorescu, M. Liserre, and A. V. Timbus, "Overview of control and grid synchronization for distributed power generation systems," *IEEE Trans. Ind. Electron.*, vol. 53, no. 5, pp. 1398–1409, Oct. 2006.
[3] P. Kundur, N. J. Balu, and M. G. Lauby, *Power System Stability and Control*, vol. 7. New York, NY, USA: McGraw-Hill, 1994.
[4] J. Fang, H. Li, Y. Tang, and F. Blaabjerg, "On the inertia of future more-electronics power systems," IEEE Trans. Emerg. Sel. Top. Power Electron., vol. 7, no. 4, pp. 2130–2146, Dec. 2019.
[5] J. Liu, Y. Miura, and T. Ise, "Comparison of dynamic characteristics between virtual synchronous generator and droop control in inverter-based distributed generators," *IEEE Trans. Power Electron.*, vol. 31, no. 5, pp. 3600–3611, May 2016.
[6] Y. Chen, R. Hesse, D. Turschner, and H.-P. Beck, "Improving the grid power quality using virtual synchronous machines," in *Proc. Int. Conf. Power Eng., Energy Elect. Drives*, 2011, pp. 1–6.
[7] J. Driesen and K. Visscher, "Virtual synchronous generators," in *Proc. IEEE Power Energy Soc. Gen. Meeting-Convers. Del. Elect. Energy 21st Century*, 2008, pp. 1–3.
[8] T. Shintai, Y. Miura, and T. Ise, "Oscillation damping of a distributed generator using a virtual synchronous generator," *IEEE Trans. Power Del.*, vol. 29, no. 2, pp. 668–676, Apr. 2014.
[9] L. Xiong *et al.*, "Static synchronous generator model: A new perspective to investigate dynamic characteristics and stability issues of grid-tied PWM inverter," *IEEE Trans. Power Electron.*, vol. 31, no. 9, pp. 6264–6280, Sep. 2016.
[10] Q.-C. Zhong and G. Weiss, "Synchronverters: Inverters that mimic synchronous generators," *IEEE Trans. Ind. Electron.*, vol. 58, no. 4, pp. 1259–1267, Apr. 2011.
[11] W. Zhang, D. Remon, I. Candela, A. Luna, and P. Rodriguez, "Grid-connected converters with virtual electromechanical characteristics: Experimental verification," *CSEE J. Power Energy Syst.*, vol. 3, no. 3, pp. 286–295, 2017.
[12] H. Wu *et al.*, "Small-signal modeling and parameters design for virtual synchronous generators," *IEEE Trans. Ind. Electron.*, vol. 63, no. 7, pp. 4292–4303, Jul. 2016.
[13] J. Chen and T. O'Donnell, "Parameter constraints for virtual synchronous generator considering stability," IEEE Trans. Power Syst., vol. 34, no. 3, pp. 2479–2481, May 2019.

[14] F. Wang, L. Zhang, X. Feng, and H. Guo, "An adaptive control strategy for virtual synchronous generator," *IEEE Trans. Ind Appl.*, vol. 54, no. 5, pp. 5124–5133, Sep./Oct. 2018.
[15] H. Wang *et al.*, "Transitioning to physics-of-failure as a reliability driver in power electronics," *IEEE Trans. Emerg. Sel. Top. Power Electron.*, vol. 2, no. 1, pp. 97–114, Mar. 2014.
[16] D. Zhou, G. Zhang, and F. Blaabjerg, "Optimal selection of power converter in dfig wind turbine with enhanced system-level reliability," *IEEE Trans. Ind Appl.*, vol. 54, no. 4, pp. 3637–3644, Jul./Aug. 2018.
[17] A. Sangwongwanich, Y. Yang, D. Sera, and F. Blaabjerg, "Mission profile-oriented control for reliability and lifetime of photovoltaic inverters," *IEEE Trans. Ind Appl.*, vol. 56, no. 1, pp. 601–610, Jan./Feb. 2020.
[18] D. Zhou, H. Wang, and F. Blaabjerg, "Mission profile based system-level reliability analysis of dc/dc converters for a backup power application," *IEEE Trans. Power Electron.*, vol. 33, no. 9, pp. 8030–8039, Sep. 2018.
[19] M. G. Pecht, D. Das, and A. Ramakrishnan, "The IEEE standards on reliability program and reliability prediction methods for electronic equipment," *Microelectron. Rel.*, vol. 42, no. 9–11, pp. 1259–1266, 2002.
[20] J. W. Harms, "Revision of MIL-HDBK-217, reliability prediction of electronic equipment," in *Proc. Annu. Rel. Maintainability Symp*., 2010, pp. 1–3.
[21] G. Zeng, C. Herold, T. Methfessel, M. Schfer, O. Schilling, and J. Lutz, "Experimental investigation of linear cumulative damage theory with power cycling test," *IEEE Trans. Power Electron.*, vol. 34, no. 5, pp. 4722–4728, May 2019.
[22] U. Choi, K. Ma, and F. Blaabjerg, "Validation of lifetime prediction of IGBT modules based on linear damage accumulation by means of superimposed power cycling tests," *IEEE Trans. Ind. Electron.*, vol. 65, no. 4, pp. 3520–3529, Apr. 2018.
[23] A. Hanif, Y. Yu, D. DeVoto, and F. Khan, "A comprehensive review toward the state-of-the-art in failure and lifetime predictions of power electronic devices," *IEEE Trans. Power Electron.*, vol. 34, no. 5, pp. 4729–4746, May 2019.
[24] J. V. M. Farias, A. F. Cupertino, V. d. N. Ferreira, H. A. Pereira, S. I. Seleme, and R. Teodorescu, "Reliability-oriented design of modular multilevel converters for medium-voltage Statcom," *IEEE Trans. Ind. Electron.*, vol. 67, no. 8, pp. 6206–6214, Aug. 2020.
[25] V. Raveendran, M. Andresen, G. Buticchi, and M. Liserre, "Thermal stress based power routing of smart transformer with CHB and DAB converters," *IEEE Trans. Power Electron.*, vol. 35, no. 4, pp. 4205–4215, Apr. 2020.
[26] N. Sintamarean, F. Blaabjerg, H. Wang, F. Iannuzzo, and P. de Place Rimmen, "Reliability oriented design tool for the new generation of grid connected PV-inverters," *IEEE Trans. Power Electron.*, vol. 30, no. 5, pp. 2635–2644, May 2015.
[27] R. Fierro and F. Lewis, "Multilayer feedforward networks are universal approximators," *IEEE Trans. Syst*., *Man, Cybern*, vol. 2, no. 5, pp. 359–366, 1989.
[28] Y. LeCun, Y. Bengio, and G. Hinton, "Deep learning," Nature, vol. 521, no. 7553, pp. 436–444, 2015.
[29] T. Dragicevic, P. Wheeler, and F. Blaabjerg, "Artificial intelligence aided automated design for reliability of power electronic systems," IEEE Trans. Power Electron., vol. 34, no. 8, pp. 7161–7171, Aug. 2019.
[30] J. He and Y. W. Li, "Analysis, design, and implementation of virtual impedance for power electronics interfaced distributed generation," *IEEE Trans. Ind. Appl.*, vol. 47, no. 6, pp. 2525–2538, Nov./Dec. 2011.
[31] X. Meng, J. Liu, and Z. Liu, "A generalized droop control for grid-supporting inverter based on comparison between traditional droop control and virtual synchronous generator control," IEEE Trans. Power Electron., vol. 34, no. 6, pp. 5416–5438, Jun. 2019.
[32] J. Fang, H. Li, Y. Tang, and F. Blaabjerg, "Distributed power system virtual inertia implemented by grid-connected power converters," *IEEE Trans. Power Electron.*, vol. 33, no. 10, pp. 8488–8499, Oct. 2018.
[33] J. M. Hogg, V. Robert and A. T. Craig, *Introduction to Mathematical Statistics*. London, U.K.: Pearson Education, 2005.
[34] "National Grid. Frequency Data for 2018," 2018. [Online]. Available: https://www.nationalgrideso.com/balancing-services/frequencyresponse- services/historic-frequency-data
[35] K. Chang, "Multiobjective optimization and advanced topics," in *Design Theory and Methods Using CAD/CAE*. New York, NY, USA: Academic, 2015, pp. 325–406.
[36] Y. P. K. G. Panchal, A. Ganatra and D. Panchal,"Behaviour analysis of multilayer perceptrons with multiple hidden neurons and hidden layers," *Int. J. Comput. Theory Eng.*, vol. 3, no. 2, pp. 332–337, 2011.
[37] D. E. Rumelhart, G. E. Hinton, and R. J. Williams, "Learning internal representations by error propagation," San Diego La Jolla Inst. Cognitive Science, California Univ., La Jolla, CA, USA, Tech. Rep. ICS 8506, 1985.
[38] "Matlab Deep Learning Toolbox." 2020. [Online]. Available: https://www.mathworks.com/products/deep-learning.html
[39] R. S. Figliola and D. E. Beasley, *Theory and Design for Mechanical Measurements*, Hoboken, NJ, USA: Wiley, 2006.

Qianwen Xu (Member, IEEE) received the B.Sc. degree from Tianjin University, Tianjin, China in 2014, and the Ph.D. degree from Nanyang Technological University, Singapore, in 2018, both in electrical engineering.

She worked as a Research Associate with Hong Kong Polytechnic University, a Postdoc Research Fellow with Aalborg University, Aalborg, Denmark, and a Wallenberg-NTU Presidential Postdoc Fellow with Nanyang Technological University. She was also a Visiting Researcher with Imperial College London, London, U.K., from March to June 2020. Currently, she is an Assistant Professor with the Department of Electric Power and Energy Systems, KTH Royal Institute of Technology, Stockholm, Sweden. Her research interests include advanced control, optimization, stability and cybersecurity of microgrids and power electronics based power systems.

Dr. Xu was the recipient of the Alexander von Humboldt Fellowship, Chinese Government Award for Outstanding Students Abroad, Excellent Doctorate Research Work in Nanyang Technological University, and the Best Paper Award in IEEE PEDG 2020.

Tomislav Dragievi (Senior Member, IEEE) received the M.Sc. and the industrial Ph.D. degrees in electrical engineering from the Faculty of Electrical Engineering, Zagreb, Croatia, in 2009 and 2013, respectively.

From 2013 to 2016, he was a Postdoctoral Research Associate with Aalborg University, Aalborg, Denmark. From March 2016 to March 2020, he was an Associate Professor with Aalborg University. Sicne April 2020, he has been a Professor with the Technical University of Denmark, Kongens Lyngby, Denmark. He made a Guest Professor stay with Nottingham University, Nottingham, U.K., during Spring/Summer of 2018. He has authored and coauthored more than 220 technical publications (more than 100 of them are published in international journals, mostly in IEEE), eight book chapters, and a book in the field. His research interests include application of advanced control, optimization and artificial intelligence inspired techniques to provide innovative and effective solutions to emerging challenges in design, control and cyber-security of power electronics intensive electrical distributions systems and microgrids.

Dr. Dragievi serves as an Associate Editor in the IEEE TRANSACTIONS ON INDUSTRIAL ELECTRONICS, IEEE TRANSACTIONS ON POWER ELECTRONICS, *IEEE Emerging and Selected Topics in Power Electronics*, and *IEEE Industrial Electronics Magazine*. He was the recipient of the Konar Prize for the Best Industrial Ph.D. thesis in Croatia, a Robert Mayer Energy Conservation Award, and is a winner of an Alexander von Humboldt Fellowship for experienced researchers. He is currently listed as one of the top five trending authors in engineering globally by Microsoft Academic.

Lihua Xie (Fellow, IEEE) received the Ph.D. degree in electrical engineering from the University of Newcastle, Callaghan NSW, Australia, in 1992.

Since 1992, he has been with the School of Electrical and Electronic Engineering, Nanyang Technological University, Singapore, where he is currently a Professor, and also Director with Delta-NTU Corporate Laboratory for Cyber-Physical Systems. He served as the Head of Division of Control and Instrumentation from July 2011 to June 2014. He held teaching appointments with the Department of Automatic Control, Nanjing University of Science and Technology, Nanjing, China, from 1986 to 1989. His research interests include robust control and estimation, networked control systems, multiagent networks, localization, and unmanned systems.

Dr Xie is an Editor-in-Chief for Unmanned Systems and an Associate Editor for IEEE TRANSACTIONS ON NETWORK CONTROL SYSTEMS. He has served as an Editor of IET Book Series in Control and an Associate Editor of a number of journals including IEEE TRANSACTIONS ON AUTOMATIC CONTROL, *Automatica*, IEEE TRANSACTIONS ON CONTROL SYSTEMS TECHNOLOGY, and IEEE TRANSACTIONS ON CIRCUITS AND SYSTEMS-II. He was an IEEE Distinguished Lecturer from January 2012 to December 2014, and an elected member of Board of Governors, IEEE Control System Society from January 2016 to December 2018). He is a fellow of IFAC and fellow of Chinese Automation Association.

Frede Blaabjerg (Fellow, IEEE) received the Ph.D. degree in electrical engineering from Aalborg University, Aalborg, Denmark, in 1995.

He was with ABB-Scandia, Randers, Denmark, from 1987 to 1988. He was an Assistant Professor in 1992, an Associate Professor in 1996, and a Full Professor of power electronics and drives in 1998. In 2017, he became a Villum Investigator. He is honoris causa with University Politehnica Timisoara (UPT), Timisoara, Romania, and Tallinn Technical University (TTU), Tallinn, Estonia. He has authored or coauthored more than 600 journal papers in the fields of power electronics and its applications. He is the co-author of four monographs and editor of ten books in power electronics and its applications. His current research interests include power electronics and its applications such as in wind turbines, PV systems, reliability, harmonics and adjustable speed drives.

Dr. Blaabjerg was the recipient of 31 IEEE Prize Paper Awards, the IEEE PELS Distinguished Service Award in 2009, the EPE-PEMC Council Award in 2010, the IEEE William E. Newell Power Electronics Award 2014, the Villum Kann Rasmussen Research Award 2014, and the Global Energy Prize in 2019. He was the Editor-in-Chief of the IEEE TRANSACTIONS ON POWER ELECTRONICS from 2006 to 2012. He has been Distinguished Lecturer for the IEEE Power Electronics Society from 2005 to 2007 and for the IEEE Industry Applications Society from 2010 to 2011 as well as from 2017 to 2018. During 2019–2020, he serves a President of IEEE Power Electronics Society. He is the Vice-President of the Danish Academy of Technical Sciences too. He is nominated during 2014–2018 by Thomson Reuters to be between the 250 most-cited researchers in engineering in the world.